nature physics

ARTICLES

PUBLISHED ONLINE: 19 DECEMBER 2010 | DOI: 10.1038/NPHYS1862

Excitable particles in an optical torque wrench

Francesco Pedaci[1†], Zhuangxiong Huang[1†], Maarten van Oene[1], Stephane Barland[2] and Nynke H. Dekker[1*]

The optical torque wrench is a laser trapping technique capable of applying and directly measuring torque on microscopic birefringent particles using spin momentum transfer, and has found application in the measurement of static torsional properties of biological molecules such as single DNAs. Motivated by the potential of the optical torque wrench to access the fast rotational dynamics of biological systems, a result of its all-optical manipulation and detection, we focus on the angular dynamics of the trapped birefringent particle, demonstrating its excitability in the vicinity of a critical point. This links the optical torque wrench to nonlinear dynamical systems such as neuronal and cardiovascular tissues, nonlinear optics and chemical reactions, all of which display an excitable binary ('all-or-none') response to input perturbations. On the basis of this dynamical feature, we devise and implement a conceptually new sensing technique capable of detecting single perturbation events with high signal-to-noise ratio and continuously adjustable sensitivity.

The past two decades have witnessed the development of new physical techniques such as atomic force microscopy, magnetic tweezers and optical tweezers that allow the mechanical manipulation and measurement of microscopic actuators. When connected to individual biomolecules, these actuators, which control physical parameters such as the applied force at the piconewton level and molecular extension at the nanometre scale, directly report on their physical properties allowing biological systems to be studied in a direct, quantitative manner in real time[1,2]. Torque is a further physical parameter of biological relevance, as witnessed by its role in diverse cellular processes such as DNA replication[3] and transcription[4], ATP synthesis[5] and bacterial propulsion[6]. For this reason, there is growing interest in the development of single-molecule techniques that allow modification and simultaneous measurement of force and torque[7–11]. To achieve this, one method is to combine the high spatio-temporal resolution of optical tweezers with the angular control of tailored microscopic birefringent particles in the so-called optical torque wrench[8,12–14] (OTW). However, although much knowledge has been gained about linear optical tweezers, its angular counterpart remains largely unexplored, a consequence of its more recent development and remaining technical challenges.

Here we focus on the fast dynamical capabilities of optical tweezers and show that the torque dynamics of the system casts the OTW within the general class of excitable dynamical systems. Both analytically and experimentally, we show that the OTW is dynamically equivalent to a microscopic version of the Adler system[15], one of the simplest and most widely studied models for the excitable spiking of a neuron[16]. Since its discovery in the seminal studies of spiking neurons[17], excitability has been identified as a feature of several nonlinear dynamical systems ubiquitous in science[18–25]. The excitable character of a system is defined by its response to external perturbations: perturbations smaller than a certain value produce a small linear response around the stable (or 'rest') state, whereas large perturbations force the system to undergo a large deterministic excursion in the phase space before returning to the stable state again. This excursion, often measured as a spike, is deterministic and independent of the perturbation, provided that it overcomes the so-called excitability threshold.

Rotational dynamics of birefringent particles

Our demonstration that the angular dynamics of a birefringent particle trapped in an OTW can be described by these physical principles starts by rotationally forcing a nano-fabricated quartz cylinder by applying a linear laser polarization rotating at constant frequency $f = \omega/2\pi$ in an OTW (Fig. 1a). The response of the mean value of the transferred torque as a function of f (Fig. 1b) clearly indicates the presence of two distinctive regimes: for frequencies $|f| < f_c^{\exp} = 35.5\,(\pm 0.5)$ Hz, the absolute value of the mean torque increases linearly with the imposed frequency; however, further increasing $|f|$ beyond $f_c^{\exp}$ results in a decay of the absolute value of the mean torque to zero (negative frequencies indicate rotation in the opposite direction). This behaviour is typical of rotationally forced systems, with optical[12,26–28], magnetic[29,30] or magneto-mechanic[24] forcing. The physical reason for the decrease of the average torque for $|f| > f_c^{\exp}$ becomes clear by looking at its temporally resolved signal: beyond the linear region (Fig. 1c), the drag torque acting on the rotating cylinder exceeds the maximum torque that can be transferred by the laser polarization, inducing a phase slip between the particle's extraordinary axis and the polarization. This event appears as a spike in the torque signal (Fig. 1d). At higher frequencies the particle is incapable of following the polarization and remains quasi-static under the scanning polarization, giving rise to a quasi-sinusoidal torque signal (Fig. 1e).

These observations can be quantitatively understood by starting from the analytical expression for the torque optically transferred to the birefringent particle, which can be written[7] as

$$\tau_{\mathrm{opt}} = -\tau_o \sin(2(\theta - \theta_o))$$

where $\tau_o = S\epsilon/(2\Omega)E_o^2 \sin(kL\Delta n)$. Here S is the particle cross-sectional area, ϵ is the permittivity, Ω is the laser optical frequency,

[1]Department of Bionanoscience, Kavli Institute of Nanoscience, Faculty of Applied Sciences, Delft University of Technology, Lorentzweg 1, 2628 CJ Delft, The Netherlands, [2]Institut Non Linéaire de Nice (UMR 6618, Université de Nice Sophia Antipolis-CNRS), 1361 Route des Lucioles, F-06560 Valbonne, France. †These authors contributed equally to this work. *e-mail: N.H.Dekker@tudelft.nl.

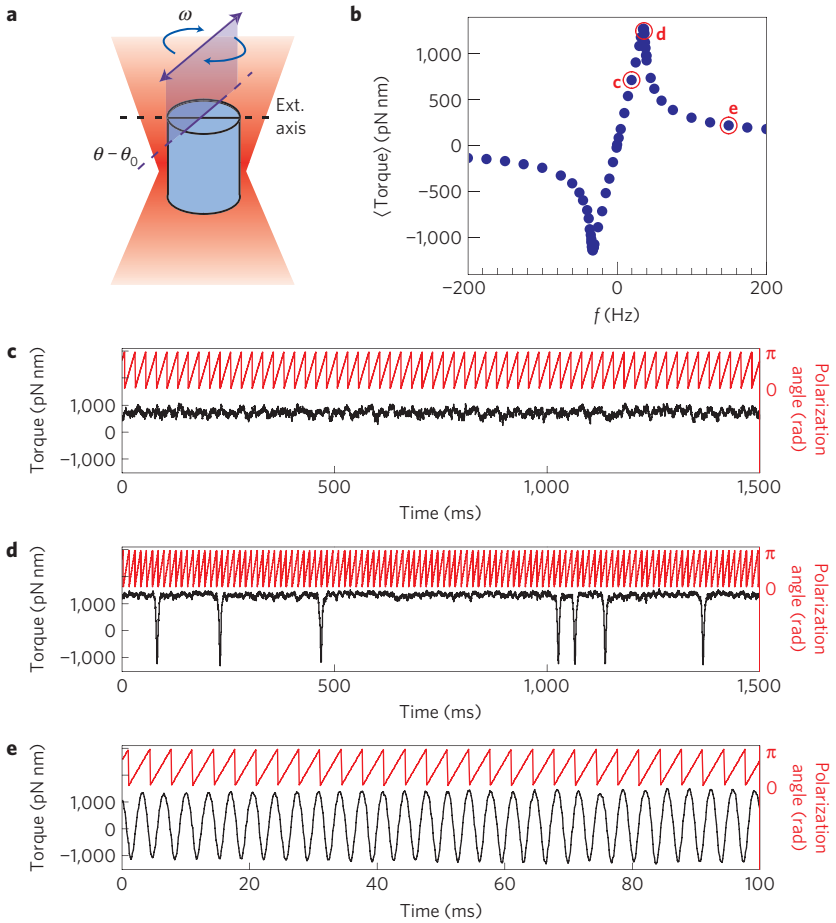

Figure 1 | Measurements of torque on a birefringent particle. a, Schematic of a birefringent cylinder forced by a rotating linear polarization in an optical trap. **b**, Mean value of the measured torque as a function of the polarization rotation frequency f. **c**–**e**, Torque as a function of time (black) corresponding to the points indicated by red circles in **b**. The relative polarization angle is depicted in red.

$\theta - \theta_o$ is the angle between the extraordinary axis of the particle (θ) and the polarization (θ_o), k is the wave vector, L is the length of the cylindrical particle, $\Delta n = 0.009$ is the quartz birefringence and a linear input polarization is assumed. When the input polarization is rotated such that $\theta_o = \omega t$, the equation of motion can be rewritten in the rotating reference frame by defining $x = \theta - \omega t$, yielding

$$\dot{x} = -\frac{\tau_o}{\gamma}\sin(2x) - \omega \qquad (1)$$

where γ is the rotational drag coefficient and where inertial effects are neglected as the Reynolds number is $\approx 10^{-4}$. Equation (1) was introduced by Adler in his seminal study of locking phenomena in oscillators[15] and is a classic example of how complex behaviour can arise from a relatively simple law.

From this equation, we expect that the behaviour of the rotationally forced microscopic system, which is periodic in x and therefore analogous to the motion of a particle on a circle, can be described in terms of the potential $V(x)$, defined as $\dot{x} = -V'(x)$ (Fig. 2). For $\omega < \omega_c = \tau_o/\gamma$, one stable and one unstable stationary solution coexist (Fig. 2, red lines and corresponding phase plots). In this regime the system is excitable: a perturbation on the stable solution that overcomes the threshold (defined by the potential barrier between the two stationary points) will be followed by a large deterministic trajectory (the 'firing state') back to the stable point (the 'resting state') in which the rotation of the particle is once more in phase with the polarization. On further increasing ω, the two stationary solutions merge through saddle-node bifurcation at $|\omega| = \omega_c$ (Fig. 2, black line and corresponding phase plot), giving rise to a limit cycle (Fig. 2, blue lines), that is, to periodic spiking at constant amplitude that is initially at infinitely low frequency and becomes sinusoidal in the limit of infinite ω (Supplementary Information SI). Thus, the observed dynamical response (Fig. 1) is captured well by the behaviour predicted by equation (1).

Experimental demonstration of excitability

To further test the validity of this model, which predicts excitability in the region $\omega < \omega_c$, we study the response of the system to controlled external perturbations (Fig. 3). Thus we first prepare the system below the critical point ($f \lesssim f_c^{\exp}$) where torque spikes are not present. A perturbation is then periodically inserted into the EOM voltage at the times indicated by red dots in the top-left time traces (Fig. 3a–c). As a result of the perturbation, the polarization phase θ_o undergoes a sudden jump (in less than 10 μs) of controlled amplitude ϕ_P ($\theta_o = \omega t + \phi_P$ with $\phi_P = [0, 1.08]$ rad). We observe that small amplitude perturbations ($\phi_P < 0.2$ rad, Fig. 3a) do not trigger torque spikes in the system's response, whereas stronger perturbations do induce torque spikes whose amplitude does not depend on the perturbation (Fig. 3b,c). The probability of triggering torque spikes rises steeply with increased perturbation amplitude (blue circles in Fig. 3d), indicating the existence of a threshold separating a 'resting' from a 'firing' state. In the right panels of Fig. 3a–c we zoom in on a collection of torque signals acquired after repeatedly imposing single perturbations triggered at $t = 0$. This shows that the response of the system to sufficiently strong perturbations varies only in the delay between the trigger and

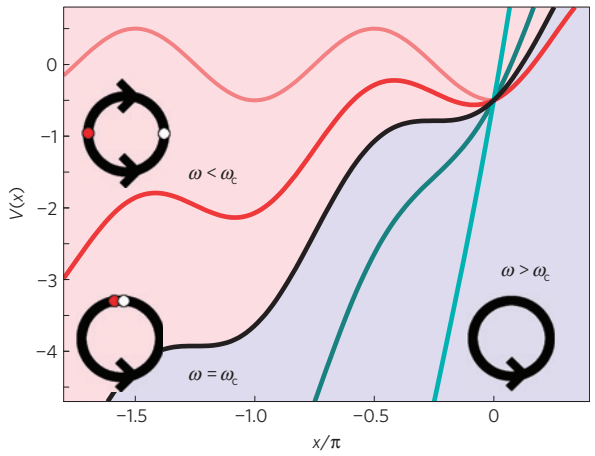

Figure 2 | The potential experienced by the birefringent particle, and corresponding phase plots. For different values of ω, we plot the potential $V(x)$ experienced by the birefringent particle ($\omega < \omega_c$, red lines; $\omega = \omega_c$, black line; $\omega > \omega_c$, blue lines) as a function of the angular coordinate in the rotating reference frame x. For these three regimes, we plot representative circular phase plots and indicate the system's fixed points by coloured dots (where a white dot represents the stable fixed point and a red dot represents the unstable fixed point). In a noise-free system, the bifurcation at $\omega = \omega_c$, evidenced by both the lack of a potential minimum and by the merging of the two fixed points in the phase plot, separates the excitable region at $\omega < \omega_c$ from the periodically modulated one at $\omega > \omega_c$. Here $\tau_o/\gamma = 1$ and $\omega = [0, 0.5, 1, 2, 6]\omega_c$ from light-red to light-blue.

the response. This delay has both a deterministic component (larger perturbations leading to shorter delay), and a stochastic one due to thermal noise (Supplementary Information SIV). Importantly, the superposition of all the excited torque spikes (Fig. 3e) reveals that the pulse shape is highly conserved even when a strong stochastic component is present in the timing, which shows that the path followed by the system during an event is deterministic, as expected for an excitable response. These measurements clearly indicate a binary ('all-or-none') response to external perturbations as well as the existence of a threshold beyond which a deterministic path drives the system back to the stable state, both characteristic features of an excitable system.

We can deepen our understanding of this physical system by modelling both the excitation probability as a function of the amplitude ϕ_P of the imposed perturbation as well as the temporal behaviour of the deterministic torque trajectory. Following previous work on stochastic effects in excitable systems[31], we derive an analytical expression for the probability to excite a torque spike as a function of the amplitude ϕ_P of the imposed perturbation (Supplementary Information SII), as

$$P(\phi_P) = \frac{1}{2}[-\mathrm{erf}(-A(\phi_P - B))] \qquad (2)$$

where $A = \sqrt{\tau_o/(2k_BT)}[1 - (\omega/\omega_c)^2]^{1/4}$, $B = \arccos(\omega/\omega_c)$ and $k_BT = 4.1$ pN nm is the thermal energy. Fitting the data in Fig. 3d with equation (2) (red line), we find that $\omega = 0.90\,\omega_c$ and $\tau_o = 1{,}150$ pN nm, where the latter is in excellent agreement with the maximum value of the torque measured experimentally (Fig. 1d,e). We note that the response of an externally driven excitable system can in general be more complex than the 1:1 locking ratio between the perturbation frequency and the system's torque spike response observed in Fig. 3d (ref. 20). The sigmoidal response observed is a particular case that can be successfully modelled by the dephasing action of thermal noise over the long perturbation period chosen (two orders of magnitude longer than the deterministic pulse duration). On reduction of the perturbation period, different locking ratios can be observed (Supplementary Information SIII). Furthermore, one can derive an expression for the deterministic trajectory of a torque spike by solving equation (1) (Supplementary Information SI), which yields

$$\frac{\tau}{\tau_0} = -\sin(2x) = \frac{\cot^2(x+\frac{\pi}{4})-1}{\cot^2(x+\frac{\pi}{4})+1} \qquad (3)$$

where $\cot(x + \pi/4) = \sqrt{(\omega_c+\omega)/(\omega_c-\omega)}[(\exp(2\sqrt{\omega_c{}^2-\omega^2}(t-t_o))-1)/(\exp(2\sqrt{\omega_c{}^2-\omega^2}(t-t_o))+1)] \simeq (\omega_c+\omega)(t-t_o)$, t_o is the time at which the peak torque is reached, and the approximation is valid when $\omega \lesssim \omega_c$. The measured torque trajectory during one 'firing' event is excellently fitted by this analytical expression, as shown by the red line in Fig. 3e.

Effects of thermal noise

Interestingly, the microscopic scale at which these experiments are carried out implies that thermal noise itself can also act as a perturbation to trigger the excitable response of the system, provided that the excitability threshold is comparable to the amplitude of thermal fluctuations. Such thermally-excited events triggered below the critical point are indeed observed (Fig. 1d). Their interspike time probability distribution, a characteristic feature of noise-driven excitable pulses[23], is shown in Fig. 4. At long time intervals, this distribution displays the typical exponential tail described by Kramer's escape rate, whereas at short time intervals the low probabilities indicate that two successive spikes are always separated by at least a minimum amount of time, proportional to the period of revolution of the polarization. This minimum time interval corresponds to the time needed for the system to return to the rest state after the emission of a spike and is termed the refractory time, t_0. For $\omega < \omega_c$, the probability distribution of interspike times is given by[31]

$$P(t) = A\tilde{W}_{tr}e^{-Kt} \qquad (4)$$

where $\tilde{W}_{tr} = \exp(-(e^{2\lambda(s-t_o)}-1)/(e^{2\lambda(t-t_o)}-1)\ln 2)(1-e^{-2\lambda(t-t_o)})^{-1/2}$, $\lambda = 2\sqrt{\omega_c{}^2-\omega^2}$, K is the Kramer decay rate, s is the midpoint of the step-like function $\tilde{W}_{tr}$, and A is a normalization constant (Supplementary Information SIV). This expression describes the experimentally-determined probability distribution very well (red line in Fig. 4).

A further effect of thermal noise is to strongly perturb the periodicity of the deterministic solution for values of ω slightly greater than ω_c, where particularly shallow regions of the potential near $x = N\pi$ render the system sensitive to thermal fluctuations[24]. As a consequence, clear periodicity is experimentally observed only for frequencies much higher than ω_c, as shown in Fig. 1e. Thus, we have clarified the origin of the nonlinear response of birefringent cylinders rotated in an optical torque wrench to perturbations, whether externally applied or of thermal origin.

Sensing through excitability

We now demonstrate the use of this excitable opto-mechanical system as a new technique for the detection of transient changes in the particle's environment (Fig. 5). In particular, we demonstrate how the rotating cylinder can detect changes in the local drag resulting from the nearby presence of objects (for example surfaces and micrometre-sized spheres), whose proximity effects can be therefore quantified. The sensing principle relies on the readout of identical torque spikes that span the entire torque range from its minimum to its maximum value, optimizing signal-to-noise. As the observation of spikes in the torque signal does not depend strongly on imperfections in the detection and calibration

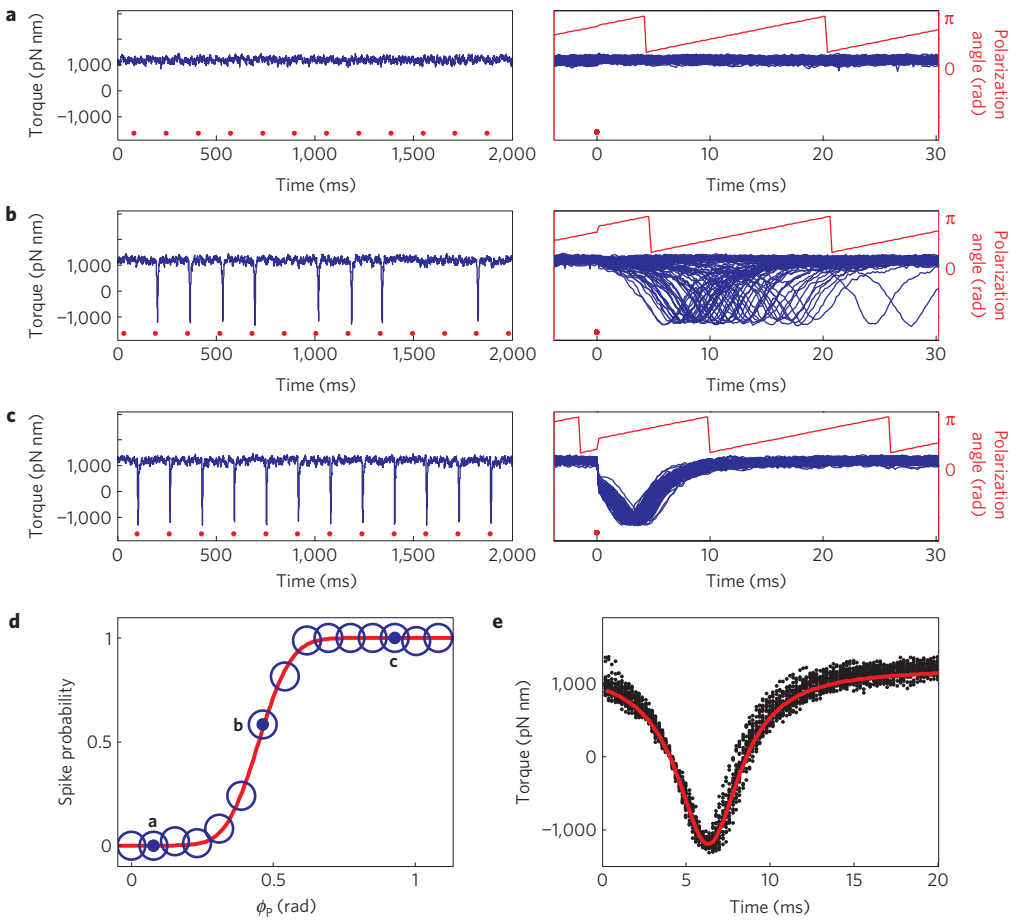

Figure 3 | Demonstration of the excitability of a rotating birefringent cylinder in an optical torque wrench. a–c (left): while keeping f fixed at 31.25 Hz, a perturbation ϕ_P is inserted into the rotating polarization at time-points indicated by the red dots, with its amplitude increasing from **a** to **c**. **a–c** (right): a zoomed-in region of the left panels, showing both the rotating polarization including its perturbation (red line) as well as the torque response (blue line). Here, the occurrence of each perturbation is defined as $t = 0$ (red line), and the torque response from a large number of collected responses is plotted. One can readily observe that the response is binary in the amplitude of the torque signal, and that the amplitude of the perturbation influences only the timing of the response. **d**, The probability of successful excitation of one spike as a function of the perturbation amplitude ϕ_P. The red line is the fit to equation (2). **e**, The superposition (dots) of the events (triggered in **b**) is fitted by equation (3) (red line), with $\tau_o = 1,200$ pN nm, $\omega_c = (2\pi)38$ rad s^{-1} and $t_o = 6.3$ ms.

(in contrast to linear detection approaches), this approach is also robust. Interestingly, as torque spikes can be excited by perturbations that overcome the excitability threshold, sensitivity can be continuously tuned by varying the threshold value, which is experimentally accessible using the parameter ω. Furthermore, we demonstrate that torque spike frequency increases with increased perturbations, a generic feature of systems that present a saddle-node bifurcation on an invariant circle (for example 'integrator' neurons, which encode the intensity of the stimulation received into their mean firing rate[16]).

By first monitoring the approach of a cylinder with respect to the bottom surface of the flow cell (Fig. 5a, red line and inset), we analyse the full spectrum of torque responses, and, in doing so, demonstrate a measurement of the local drag encountered by the cylinder (Fig. 5a–d). Setting $\omega < \omega_c^{exp}$ so that the isolated excitable cylinder will be insensitive to thermal fluctuations, we record both the position of the cylinder in the optical trap (Fig. 5a, blue points) and the corresponding torque signal (Fig. 5b). When the cylinder is far from the surface, it is located at the trap centre and the torque signal is initially featureless. However, as the cylinder approaches the surface, torque spikes make their appearance (Fig. 5b, region near 8 s). Subsequently, as the cylinder starts to enters into contact with the surface (at the positions indicated by dashed grey lines in Fig. 5a–d), it is displaced relative to the centre of

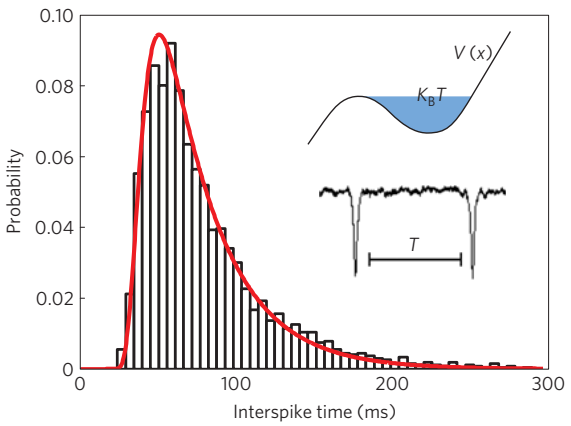

Figure 4 | Probability distribution for the interspike time of events triggered by thermal noise. Here, the value of f (34.5 Hz) is selected such that the excitability threshold is readily overcome by thermal events (see sketch of the potential $V(x)$ and of the torque interspike time T in the inset). The red line fits the data using equation (4) with $s = 42$ ms, $t_o = 13$ ms, $\lambda = 60$ Hz, $K = (35$ ms$)^{-1}$. The observed probability distribution also confirms the negligible role of inertia in the dynamics of this system, as otherwise a second peak would become observable[31].

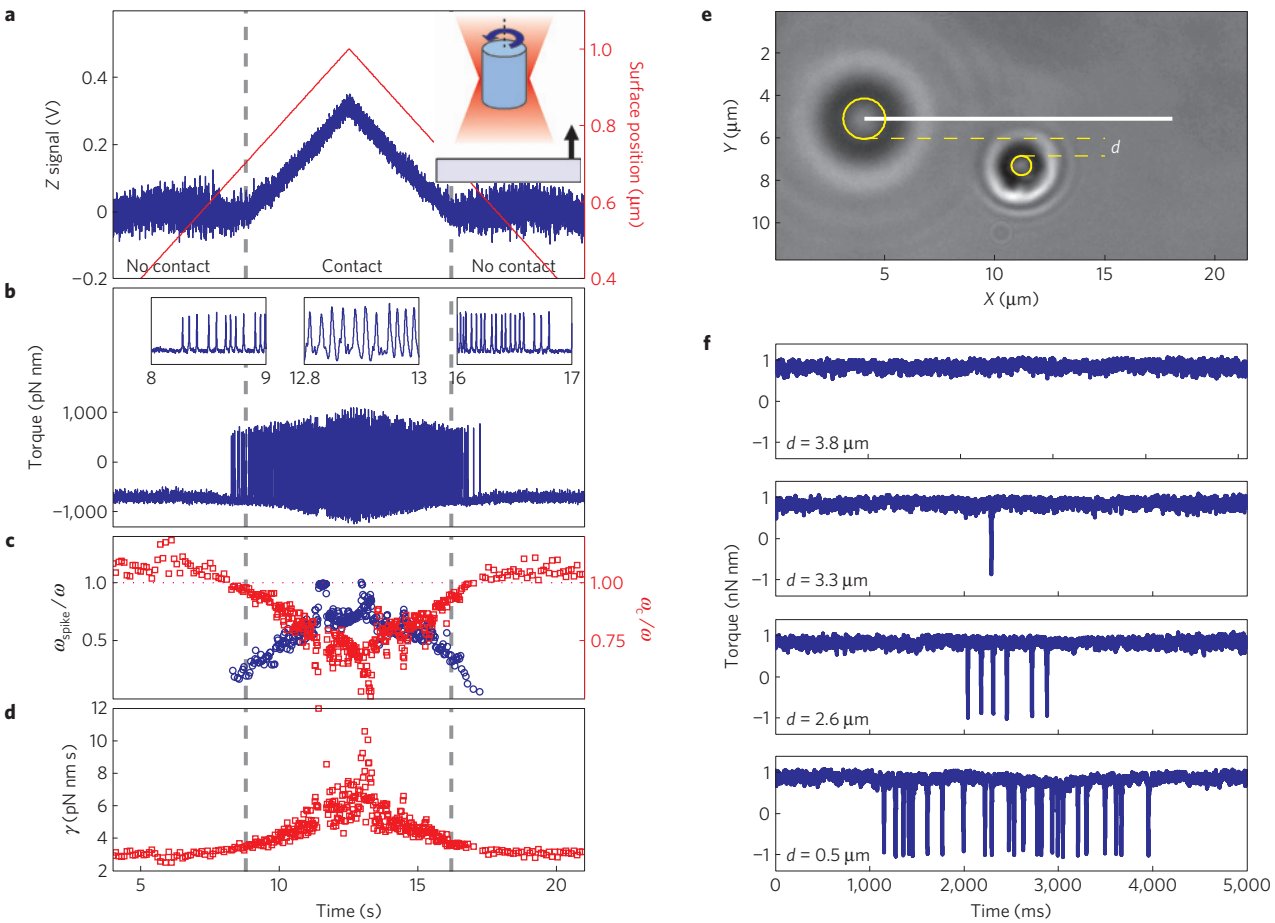

Figure 5 | Sensing through excitability. a–d, Vertical motion of the excitable particle towards a surface (followed by its reverse trajectory). **a**, A trapped birefringent cylinder is constantly rotated at a sub-critical frequency ($\omega/2\pi = 35$ Hz, 80% of ω_c measured in bulk) while the trap is approached towards the glass surface of the flow cell (inset). The relative distance of the trap from the surface is shown in red. The recorded signal of the vertical displacement of the cylinder from the trap centre is shown in blue and its deviations from zero indicate contact with the surface, in which the particle exerts a restoring force on the surface of maximally a few piconewtons. **b**, Torque signal recorded during the vertical movement. Insets: Zooms of the trace at three different points along the trajectory and its reversal; timescales for zooms are indicated in seconds. **c**, (Blue points) Ratio of the measured quasi-instantaneous spike frequency and polarization rotation ω. An increase in this ratio corresponds to a decrease in ω_c or equivalently an increase in drag. Transient sticking to the surface (or equivalently a transiently infinite drag) is visible at the points where this ratio becomes equal to 1. (Red points) Ratio of the measured critical frequency $\omega_c(z)$ and the polarization rotation frequency ω. The critical frequency can be deduced from the torque signal in **b**, both before and after the bifurcation at $\omega_c/\omega = 1$ (Supplementary Information SVII). **d**, Rotational drag along the trajectory, calculated using the value of ω_c in **c**. **e**,**f**, Sensing a moving object through proximity effects. **e**, A 2 μm diameter bead fixed to the glass surface (large yellow circle, left) is moved at constant speed along the white line, while the excitable cylinder (small yellow circle, right) is kept in rotation at a sub-critical frequency. **f**, The torque traces along the path are shown for different values of distance d. Proximity effects (for example transient increases of the drag coefficient) effectively lower the potential barrier, which keeps the rotation of the cylinder in phase with the laser polarization, translating into large torque spikes. For all figure panels, we have fixed the maximum applicable torque τ_o as well as the cylinder rotation frequency ω dictated by the EOM.

the optical trap (Fig. 5a, blue points in region labelled 'contact'). These torque spikes report on the occurrence of the bifurcation in this excitable system (that is $\omega = \omega_c$). Their frequency, ω_{spike}, depends on the relative distance between the rotating cylinder and the surface (Fig. 5b, blue spikes in insets). By local averaging, we determine the dependence of the nearly-instantaneous spike frequency ω_{spike} on the relative distance from the surface (Fig. 5c, blue points), which illustrates that ω_{spike} approaches ω as the cylinder is pressed into the surface.

The varying character of the torque spikes as the cylinder approaches a surface can be understood as follows. First, the spike frequency encodes information on the system's critical frequency, $\omega_c(z)$: specifically, $\omega_{spike} \propto \sqrt{\omega^2 - \omega_c(z)^2}$ (Supplementary Information SI). As the cylinder is brought into contact with the surface, the system's critical frequency decreases, becoming equal to ω and then dropping beneath it (Fig. 5c, red points). Hence, the torque signal displays thermally excited spikes when the cylinder is close to the surface (where $\omega \simeq \omega_c(z)$) and periodic spikes when it is pressed into tight contact with the surface (where $\omega \gg \omega_c(z)$).

We can use the relationship $\gamma(z) = \tau_o/\omega_c(z)$ to determine how the drag γ varies with the relative position of the particle and the surface (Fig. 5d). According to Faxén's law, the rotational drag should increase in the vicinity of a surface[32], as observed (Fig. 5d, regions before contact indicated by grey lines). Further increase of the drag is measured as the cylinder is brought into contact with the surface and the pressure is increased. As the measurement of the drag (Fig. 5d) and the position signal (Fig. 5a) demonstrate, we do not observe permanent sticking of the particle after contact is reached, probably as a result of the proteinaceous coating applied to the inner flow cell surfaces in these experiments.

This well-understood sensitivity of the torque signal to changes in the local drag can be employed for the detection of particles in the

cylinder's vicinity. To demonstrate this, we employ a polystyrene bead (2 μm diameter, large yellow circle in Fig. 5e) fixed to the glass surface as the source of the perturbation and scan the microscope piezo-stage at constant velocity (over a total distance of 14 μm along x, white line in Fig. 5e), thereby simulating the presence of a flow-driven bead in the sensor's proximity. While doing so, we control the lateral distance d (along y) between the surfaces of the cylinder and the bead, while the trap is maintained $\simeq$2 μm from the glass surface. As above, we select $\omega < \omega_c^{exp}$ and record the torque signal during the movement of the stuck bead for decreasing values of d.

As shown in the temporal traces (Fig. 5f), the proximity of the bead can be easily recognized from the appearance of spikes, which are excited in a region where the distance between the bead and the cylinder is minimized. As expected, such a response by the cylinder to an approaching object is observed only in the nonlinear regime: when ω is reduced so as to induce a linear response, spikes are absent and only a barely visible perturbation of the torque signal is visible (data not shown). As such, a rotating birefringent particle can be employed as a sensitive nonlinear detector, whereby spatial localization of the sensor is assured with great accuracy by the three-dimensional optical trap and its sensitivity exploits the sensor's excitable character.

Methods

To constitute the optical trap, the laser light (100 mW at a wavelength of 1,064 nm) is focused by a 1.49 NA objective in a glass flow cell mounted on piezo-actuators. We use a fast (~MHz) electro-optical modulator (EOM) in combination with a quarter-wave plate as a polarization control system[14]. As a result, the angle of the linear polarization of the trapping laser field (ellipticity smaller than 5%) is proportional to the voltage applied to the EOM in the angular range 0–π. To continuously rotate the polarization at a constant rate $f = \omega/2\pi$, we use a sawtooth voltage signal of controlled frequency $2f$. The torque transferred to the trapped particle is measured optically by fast intensity detectors from the imbalance of the two circular components of the polarization at the output of the trap[7]. The total bandwidth of the detection system is 200 kHz, which readily allows sensitive torque detection on sub-millisecond timescales and is key to our experiments. An input polarization reference and a calibration procedure (similar to the one carried out for linear optical tweezers[12,33]) are necessary to obtain the absolute value of the applied torque in physical units. The birefringent particles employed are cylinders of slightly conical shape (1.7 μm height, 0.9 μm larger diameter, 0.6 μm smaller diameter), obtained by electron beam lithography on a quartz wafer. The advantage of this technique over optical lithography[13] lies in its finer control over dimensions and accuracy. A detailed description of cylinder fabrication will be published elsewhere (Z.H. *et al.*, manuscript in preparation). The glass surface of the flow cell is coated with BSA proteins immobilized by use of a nitrocellulose layer, to prevent sticking with the quartz surface of the particles. The 2 μm bead is stuck to the glass surface via the nitrocellulose layer.

Received 8 July 2010; accepted 25 October 2010; published online 19 December 2010

References

1. Neuman, K. C. & Nagy, A. Single-molecule force spectroscopy: Optical tweezers, magnetic tweezers and atomic force microscopy. *Nature Methods* **5,** 491–505 (2008).
2. Bustamante, C., Macosko, J. & Wuite, G. Grabbing the cat by the tail: Manipulating molecules one by one. *Nat. Rev. Mol. Cell Biol.* **1,** 130–136 (2000).
3. Funnell, B. E., Baker, T. A. & Kornberg, A. *In vitro* assembly of a prepriming complex at the origin of the Escherichia coli chromosome. *J. Biol. Chem.* **262,** 10327–10334 (1987).
4. Liu, L. F. & Wang, J. C. Supercoiling of the DNA template during transcription. *Proc. Natl Acad. Sci. USA* **84,** 7024–7027 (1987).
5. Yoshida, M., Muneyuki, E. & Hisabori, T. ATP synthase, a marvellous rotary engine of the cell. *Nat. Rev. Mol. Cell Biol.* **2,** 669–677 (2001).
6. Sowa, Y. & Berry, R. M. Bacterial flagellar motor. *Q. Rev. Biophys.* **41,** 103–132 (2008).
7. Friese, M. E. J., Nieminen, T. A., Heckenberg, N. & Rubinsztein-Dunlop, H. Optical alignment and spinning of laser-trapped microscopic particles. *Nature* **394,** 348–350 (1998).
8. Forth, S. *et al.* Abrupt buckling transition observed during the plectoneme formation of individual DNA molecules. *Phys. Rev. Lett.* **100,** 148301 (2008).
9. Bryant, Z. *et al.* Structural transitions and elasticity from torque measurements on DNA. *Nature* **424,** 338–341 (2003).
10. Celedon, A. *et al.* Magnetic tweezers measurement of single molecule torque. *Nano Lett.* **9,** 1720–1725 (2009).
11. Lipfert, J., Kerssemakers, J. W. J., Jager, T. & Dekker, N. H. Magnetic torque tweezers: Measuring torsional stiffness in DNA and RecA-DNA filaments. *Nature Methods* published online doi:10.1038/nmeth.1520, (17 October 2010).
12. La Porta, A. & Wang, M. D. Optical torque wrench: Angular trapping, rotation, and torque detection of quartz microparticles. *Phys. Rev. Lett.* **92,** 190801 (2004).
13. Deufel, C., Forth, S., Simmons, C. R., Dejgosha, S. & Wang, M. D. Nanofabricated quartz cylinders for angular trapping: DNA supercoiling torque detection. *Nature Methods* **4,** 223–225 (2007).
14. Gutierrez-Medina, B., Andreasson, J. O. L., Greenleaf, W. J., La Porta, A. & Block, S. M. An optical apparatus for rotation and trapping. *Methods Enzymol.* **475,** 377–404 (2010).
15. Adler, R. A study of locking phenomena in oscillators. *Proc. IRE* **34,** 351–357 (1946).
16. Izhikevich, E. M. Neural excitability, spiking and bursting. *Int. J. Bifurc. Chaos* **10,** 1171–1266 (2000).
17. Hodgkin, A. L., Huxley, A. F. & Katz, B. Measurement of current–voltage relations in the membrane of the giant axon of Loligo. *J. Physiol.* **116,** 424–448 (1952).
18. Rush, A. M. *et al.* A single sodium channel mutation produces hyper- or hypoexcitability in different types of neurons. *Proc. Natl Acad. Sci. USA* **103,** 8245–8250 (2006).
19. Izhikevich, E. M. *Dynamical Systems in Neuroscience* (MIT Press, 2006).
20. Feingold, M., Gonzalez, D. L., Piro, O. & Viturro, H. Phase locking, period doubling, and chaotic phenomena in externally driven excitable systems. *Phys. Rev. A* **37,** 4060–4063 (1988).
21. Glass, L., Hunter, P. & McCulloch, A. *Theory of Heart: Biomechanics, Biophysics, and Nonlinear Dynamics of Cardiac Function* (Springer, 1991).
22. Barland, S., Piro, O., Giudici, M., Tredicce, J. R. & Balle, S. Experimental evidence of van der Pol–Fitzhugh–Nagumo dynamics in semiconductor optical amplifiers. *Phys. Rev. E* **68,** 036209 (2003).
23. Yacomotti, A. M. *et al.* Interspike time distribution in noise driven excitable systems. *Phys. Rev. Lett.* **83,** 292–295 (1999).
24. Coullet, P., Gilli, J. M., Monticelli, M. & Vandenberghe, N. A damped pendulum forced with a constant torque. *Am. J. Phys.* **73,** 1122–1128 (2005).
25. Epstein, I. R. & Pojman, J. A. *An Introduction to Nonlinear Chemical Dynamics: Oscillations, Waves, Patterns, and Chaos* (Oxford Univ. Press, 1998).
26. Shelton, W. A., Bonin, K. D. & Walker, T. G. Nonlinear motion of optically torqued nanorods. *Phys. Rev. E* **71,** 036204 (2005).
27. Rothmayer, M., Tierney, D., Frins, E., Dultz, W. & Schmitzer, H. Irregular spin angular momentum transfer from light to small birefringent particles. *Phys. Rev. A* **80,** 043801 (2009).
28. Rodriguez-Otazo, M., Augier-Calderin, A., Galaup, J-P., Lamère, J-F. & Fery-Forgues, S. High rotation speed of single molecular microcrystals in an optical trap with elliptically polarized light. *Appl. Opt.* **48,** 2720–2730 (2009).
29. McNaughton, B. H., Agayan, R. R., Clarke, R., Smith, R. G. & Kopelman, R. Single bacterial cell detection with nonlinear rotational frequency shifts of driven magnetic microspheres. *Appl. Phys. Lett.* **91,** 224105 (2007).
30. Helgesen, G., Pieranski, P. & Skjeltorp, A. T. Nonlinear phenomena in systems of magnetic holes. *Phys. Rev. Lett.* **64,** 1425–1428 (1990).
31. Eguia, M. C. & Mindlin, G. B. Distribution of interspike times in noise-driven excitable systems. *Phys. Rev. E* **61,** 6490–6499 (2000).
32. Leach, J. *et al.* Comparison of Faxén's correction for a microsphere translating or rotating near a surface. *Phys. Rev. E* **79,** 026301 (2009).
33. Tolić-Norrelykke, S. F. *et al.* Calibration of optical tweezers with positional detection in the back focal plane. *Rev. Sci. Instrum.* **77,** 103101 (2006).

Acknowledgements

We thank A. La Porta for graciously sharing key aspects of the construction of OTW, M. Wang for discussion of polarization, E. van der Drift, M. Zuiddam, A. van Run and M. van der Krogt of the Delft Nanofacility and J. Andreasson of Stanford University for advice on the microfabrication of quartz cylinders, M. Wiggin for help in fabricating them, J. van der Does, D. de Roos and J. Beekman for help with instrumentation and infrastructure, J. Kerssemakers, I. de Vlaminck, M. van Loenhout, S. Klijnhout and J. Lipfert for stimulating discussions, and the TU Delft, FOM (Dutch Foundation for Research on Matter), NWO (Nederlandse Organisatie voor Wetenschappelijk Onderzoek) and the European Science Foundation for financial support.

Author contributions

F.P. and Z.H. contributed equally to this work. F.P., S.B. and N.H.D. conceived and designed the experiments. F.P., M.v.O. carried out the experiments. Z.H. developed the nanofabrication protocols. F.P., Z.H., S.B. and M.v.O. analysed the data. Z.H. and S.B. contributed materials and analysis tools. F.P., Z.H., S.B. and N.H.D. wrote the paper.

Additional information

The authors declare no competing financial interests. Supplementary information accompanies this paper on www.nature.com/naturephysics. Reprints and permissions information is available online at http://npg.nature.com/reprintsandpermissions. Correspondence and requests for materials should be addressed to N.H.D.